XLVI CILAMCE
VITÓRIA - ES - BRAZIL - 2025
XLVI IBERO-LATIN AMERICAN CONGRESS ON COMPUTATIONAL METHODS IN ENGENEERING

Shape factors for irregular apertures via high-order polynomial reconstruction and a Galerkin-based integral formulation

Valdecir A. S. Júnior[1], Juan Galvis[2], Gustavo P. Oliveira[3]

[1]*Department of Physics and Civil Engineering, State University of Paraíba, Araruna, Brazil*
[2]*Department of Mathematics, Universidad Nacional de Colombia, Bogotá D.C., Colombia*
[3]*Departament of Scientific Computing, Federal University of Paraíba, João Pessoa, Brazil*

asjrvaldecir@servidor.uepb.edu.br, jcgalvisa@unal.edu.co, gustavo.oliveira@ci.ufpb.br

Abstract. This study presents a Galerkin-based integral (GBI) method for computing shape factors in cross-sections bounded by irregular geometries, as commonly found in fractured systems. The approach combines high-order piecewise polynomial reconstruction of the aperture boundary with a semi-analytical formulation based on weighted residuals to solve the governing flow equations under laminar conditions. A set of three realistic geometries, obtained from fractures in cylindrical concrete specimens, was used to evaluate the method's performance. Results include velocity fields, Poiseuille numbers, and shape factors, all computed with high accuracy and low computational cost. Validation against finite element solutions implemented in `FEniCSx/DolfinX` shows excellent agreement across all tested cases, confirming the robustness and precision of the GBI method. Despite minor discontinuities at subdomain interfaces, the computed hydraulic quantities remain consistent and reliable. The proposed methodology offers a computationally efficient alternative to traditional discretization techniques for modeling transport phenomena in porous or fractured media.

Keywords: Porous media, Pore characterization, Galerkin-based integral method, Computational fluid dynamics

1 Introduction

Understanding fluid transport in fractured and porous domains is essential in many scientific and engineering applications, where internal discontinuities—whether natural or artificially induced—govern flow behavior. These voids, referred to as apertures, appear in contexts as diverse as subsurface hydrology, construction materials [1], biomedical sealing systems [2], and carbon storage technologies [3]. Although experimental techniques have advanced in mapping aperture profiles [4–6], the influence of irregular cross-sectional geometries on fluid dynamics remains only partially understood.

Classical formulations, such as the Kozeny–Carman equation [7, 8], are not well suited to capture the heterogeneity and nonlinearity inherent in real domains. Several authors [9–12] emphasize the limitations of conventional geometric metrics in correlating porosity and permeability, especially when complex shapes are involved. Similarly, numerical strategies such as discrete fracture networks [13] and finite difference methods [14] often fall short in deriving shape factors for domains bounded by irregular contours.

This study presents a Galerkin-based integral (GBI) model to compute shape factors in apertures with arbitrary boundaries, combining high-order boundary reconstruction with simulations based on the Poiseuille number [15–17]. The analysis is performed on fractures formed in cylindrical concrete specimens under controlled conditions following the numerical perspective introduced by the authors in earlier papers [18–20]. The induced fissures share morphological characteristics with those in rock core plugs used for oil and gas studies, which supports the model's relevance to petroleum applications, where such geometries critically influence reservoir flow modeling, especially matrix acidizing in anticipation to enhanced recovery or geological carbon storage processes.

2 Methodology

The methodology developed in this work estimates flow behavior within the irregular apertures using a weighted-residual approach. It begins with the geometric reconstruction of the domain's boundary and proceeds to

the numerical solution of the governing flow equations, ultimately yielding a representative shape factor.

2.1 Definitions and approximation

To represent the cross-sectional geometry of the aperture, we define the domain $\Omega \subset \mathbb{R}^2$ as the region bounded below and above by continuous curves $\psi_I(x_1)$ and $\psi_S(x_1)$, respectively. The distance $\delta(x_1) = \psi_S(x_1) - \psi_I(x_1)$ characterizes the local vertical opening. This representation allows us to describe complex geometries through a series of piecewise polynomial approximations over a partition $\Delta = \{a_i\}_{i=1}^{n}$ of the domain in the x_1 direction.

Each segment $\Delta_i = [a_{i-1}, a_i]$, $i = 1, ..., n$, is associated with a local polynomial $P_{c,i} = \sum_{q=0}^{k_i} g_{c,i,q} x_1^q$, for $g_{c,i,q} \in \mathbb{R}$, where $c = I, S$ and $k_i \leq k$, is the degree of $P_{c,i}$, $i = 1, ..., n.$, approximating either ψ_I or ψ_S. These polynomials are built as linear combinations of monomials x_1^q of varying degrees k_i. The collection of all $P_{c,i}$ polynomials forms an accurate reconstruction of the aperture's geometry. Figure1 illustrates this procedure.

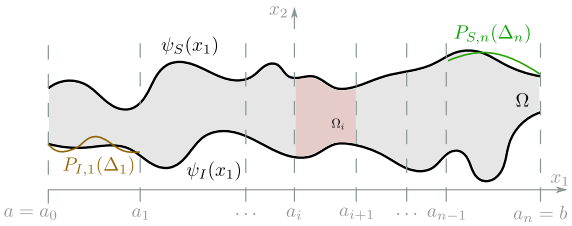


Figure 1. Aperture's mathematical model: the domain is bounded above and below by continuous curves (ψ_I and ψ_S) separated by varying displacements. The partition knots a_i allow us to approximate the boundary curves by univariate piecewise polynomials.

2.2 Mathematical framework

The flow considered in this work is laminar, steady, incompressible and driven by a constant pressure gradient through the aperture. The velocity component $u(x_1, x_2)$ in the axial direction x_3 satisfies the Poisson equation:

$$\mu \nabla^2 u + \frac{dp}{dx_3} = 0 \quad \text{in } \Omega, \quad u = 0 \quad \text{on } \partial\Omega, \tag{1}$$

where μ is the dynamic viscosity, and $\frac{dp}{dx_3}$ is the constant pressure gradient driving the flow in the axial direction.

To isolate geometric effects, the problem is reformulated in dimensionless form using a characteristic length l. The dimensionless velocity u^* satisfies:

$$\nabla^2 u^* = -1 \quad \text{in } \Omega, \; u^* = 0 \quad \text{on } \partial\Omega. \tag{2}$$

This equation is solved using a Galerkin-based integral (GBI) method. The solution u^* is approximated as a linear combination of basis functions $w_{j,i}(x_1, x_2)$, which are constructed from the product of a support function and bivariate monomials:

$$w_{j,i}(x_1, x_2) = \phi_i(x_1, x_2) \cdot \Phi_{\alpha_1 \alpha_2}(x_1, x_2), \quad j = 1, \ldots, J. \tag{3}$$

Here, the support function is defined as:

$$\phi_i(x_1, x_2) = (P_{I,i} - x_2)(P_{S,i} - x_2), \quad \text{for } (x_1, x_2) \in \Omega_i, \tag{4}$$

which vanishes at the domain boundaries, and the monomials are:

$$\Phi_{\alpha_1 \alpha_2}(x_1, x_2) = x_1^{\alpha_1} x_2^{\alpha_2}, \quad \text{with } |\alpha| \leq m, \tag{5}$$

where $m < \infty$ is a user-defined accuracy parameter. As m increases, the space of basis functions expands, leading to improved approximation of the exact PDE solution.

Each basis function $w_{j,i}$ can be explicitly written as:

$$\begin{aligned} w_{1,i} &= \phi_i \Phi_{00} = \phi_i x_1^0 x_2^0 \\ w_{2,i} &= \phi_i \Phi_{10} = \phi_i x_1^1 x_2^0 \\ w_{3,i} &= \phi_i \Phi_{01} = \phi_i x_1^0 x_2^1 \\ w_{4,i} &= \phi_i \Phi_{11} = \phi_i x_1^1 x_2^1 \\ w_{5,i} &= \phi_i \Phi_{20} = \phi_i x_1^2 x_2^0 \\ w_{6,i} &= \phi_i \Phi_{02} = \phi_i x_1^0 x_2^2 \\ \vdots & \qquad \vdots \\ w_{j,i} &= \phi_i \Phi_{\alpha_p \alpha_q} \end{aligned}$$

The approximation over each subdomain Ω_i is:

$$u\Big|_{\Omega_i} \approx \hat{u}_i = \sum_{j=1}^{J} c_j w_{j,i}. \tag{6}$$

This expansion is used in the Galerkin formulation, where the residual of the PDE is integrated against each test function w_k over its respective subdomain:

$$\int_{\Omega_i} \nabla u^* \cdot \nabla w_k \, d\Omega = \int_{\Omega_i} w_k \, d\Omega. \tag{7}$$

Local systems are assembled into a global linear system $\mathbf{Mc} = \mathbf{b}$, with stiffness matrix $\mathbf{M}$ and load vector $\mathbf{b}$. The coefficients $\mathbf{c}$ allow for the reconstruction of the approximate velocity u^* across the domain.

Once the velocity field is known, the Poiseuille number can be computed as:

$$Po = \frac{d_h^2}{2\overline{u}^*}, \tag{8}$$

where d_h is the hydraulic diameter and $\overline{u}^*$ is the mean dimensionless velocity. The dimensionless shape factor is then defined by:

$$F_{val} = \frac{Po}{8}. \tag{9}$$

This parameter quantifies the geometric resistance to internal flow. Unlike conventional factors for simple shapes, F_{val} can be consistently evaluated for irregular cross-sections using the present GBI method. This formulation follows the approach proposed in [19] for shape factor estimation via the Poiseuille number.

To compute the shape factors, the geometric attributes, namely area A, perimeter p, and hydraulic diameter d_h^*, were obtained through numerical integration over the reconstructed domains and their boundaries. The corresponding expressions are:

$$A_i = \int_{\Omega_i} (P_{S,i} - P_{I,i}) \, d\Omega_i, \tag{10a}$$

$$\mathrm{p}_i = \sum_c \int_{\partial\Omega_i} \left[1 + \left(\frac{dP_{c,i}}{dx_1} \right)^2 \right]^{1/2} dx_1, \quad c = S, I, \tag{10b}$$

$$d_{h,i}^* = \frac{4A_i}{\mathrm{p}_i}, \text{ and} \tag{10c}$$

$$A = \sum_i A_i, \quad \mathrm{p} = \sum_i \mathrm{p}_i, \quad d_h^* = \sum_i d_{h,i}^*, \quad \text{for } i = 1, \ldots, n. \tag{10d}$$

3 Results and discussion

3.1 Boundary reconstruction and shape factor computation

To demonstrate the capability of the proposed method in computing shape factors for arbitrary geometries, three distinct apertures corresponding to surface fractures were selected. These fractures were generated from cylindrical concrete specimens with dimensions of 10×20 cm (diameter and height, respectively) ruptured under controlled uniaxial compression at approximately 1 MPa to induce cracking (Fig. 2). After rupture, the internal fracture surfaces were exposed and digitally captured for further analysis (Fig. 3).



Figure 2. Fracture generation experiment: compression apparatus (left); cylindrical concrete specimen (middle); fractures molded according to NBR 5738 – the Brazilian regulation for test specimen preparation [21] – ruptured under compression after 28 days of submerged curing.



Figure 3. Top-view images of the upper fracture surfaces of cylindrical concrete specimens after rupture.

The accuracy of the geometric reconstruction was controlled by the parameter m, whose maximum value was set to 6. This parameter was adjusted based on the local curvature complexity observed in each aperture profile. The number of upper and lower curves (i.e., subdomain partitions) was chosen to closely approximate the actual fracture geometry. By increasing the number of partitions n, the approximation of the reconstructed curves toward the real boundary improves; however, $10 \leq n \leq 20$ provides a sufficiently accurate representation without significant loss in the computed velocity values. The adopted subdomain segmentation strategy ensured accurate representation of key geometric features while maintaining consistency with subsequent numerical procedures, particularly those involving integration over the domain and its boundaries.

To characterize the flow behavior, the dimensionless axial velocity field u^* was computed, oriented upward and perpendicular to the plane of the figure. The resulting velocity contours exhibit the typical parabolic profile associated with laminar flow between parallel boundaries, with velocity peaks at the central region and minima near the walls, as expected under homogeneous Dirichlet boundary conditions. The computed velocity field responds sensitively to local geometrical variations, accelerating in wider regions and decelerating in narrower sections of the aperture. Contour plots were included to enhance the visualization of these flow patterns (Fig. 4b).

Table 1 summarizes the geometric and hydraulic parameters computed for each aperture, including the cross-sectional area A, perimeter p, dimensionless hydraulic diameter d_h^*, average axial velocity $\overline{u}^*$, Poiseuille number (Po), and the resulting shape factor F_{val}. The value of $\overline{u}^*$ was obtained directly from the simulated velocity field.

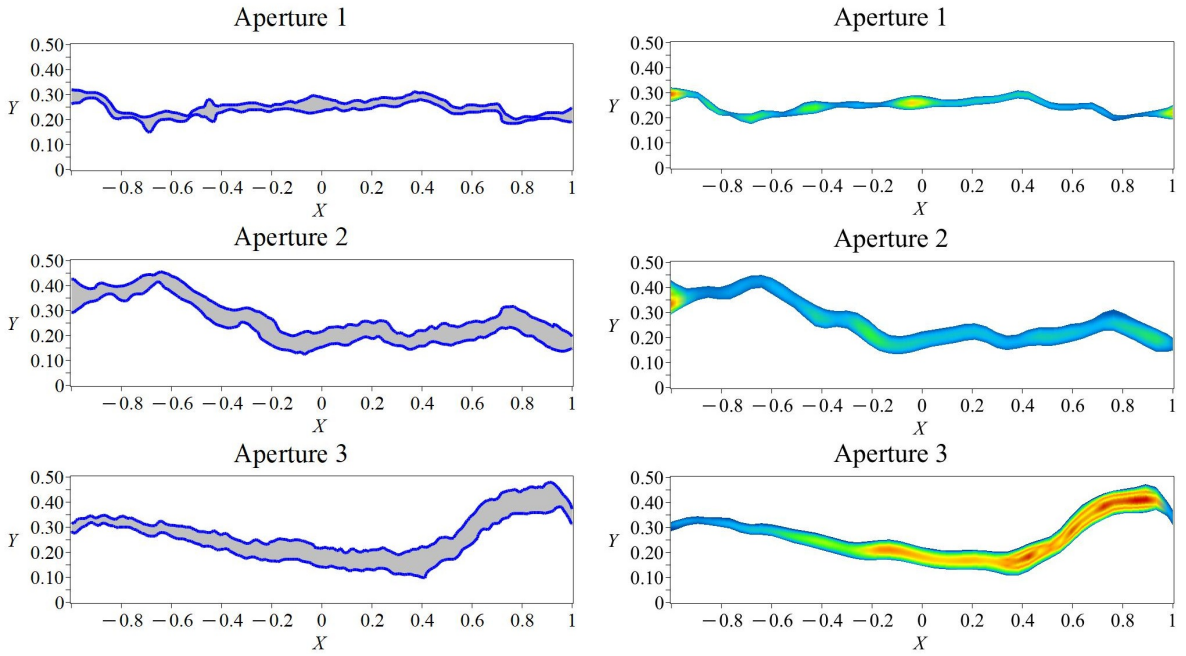


Figure 4. Aperture reconstruction: geometric boundaries approximated by piecewise polynomial fitting (left column); velocity contours, where reddish tones indicate local peaks and regions of higher velocity (right column).

Table 1. Geometric and hydraulic parameters computed for each aperture using the GBI method.

Aperture	A	p	d_h^*	$\overline{u^*}$	Po	F_{val}
1	0.0600	4.5001	0.05333	9.01e-04	15.8024	1.9753
2	0.1105	4.7812	0.09244	3.242e-4	13.1798	1.6475
3	0.1348	4.5732	0.11790	4.69e-04	14.7918	1.8489

3.2 Validation from finite element results

Since theoretical references for general shape factors are unavailable. the governing boundary value problem was independently solved using the `FEniCSx/DolfinX`[1] finite element (FE) framework to validate the results produced by the GBI method. `FEniCSx` is an open-source platform for solving partial differential equations via the finite element method, with full integration in Python and support for high-performance linear algebra backends.

The boundary value problem described in Eq. 2 was implemented and solved in `FEniCSx` for all aperture models. The computational domains were discretized using two-dimensional triangular meshes with Lagrange P_1 elements supported by the software's own symbolic language to derive the variational formulation. Linear systems were resolved using PETSc solvers with the Generalized Minimal Residual (GMRES) method and appropriate preconditioning strategies.

For each aperture, the dimensionless velocity field, the average velocity $\overline{u}^*$, the hydraulic diameter d_h^*, the cross-sectional area A, the perimeter p, the Poiseuille number Po, and the resulting shape factor F_{val} were calculated. These values are presented in Table 2. Figure 5 illustrates the dimensionless velocity fields simulated using the finite element method for the four analyzed apertures. The same parameters were independently derived from the FE simulations in `FEniCSx/DolfinX` and compared to the corresponding GBI outputs.

The comparison confirms that the shape factors F_{val} obtained with the FEniCSx simulations match closely with those computed through the GBI approach. This consistency supports the validity of both implementations and highlights the effectiveness of the GBI method for estimating shape factors in irregular fracture geometries.

[1]Available at `https://github.com/FEniCS/dolfinx`

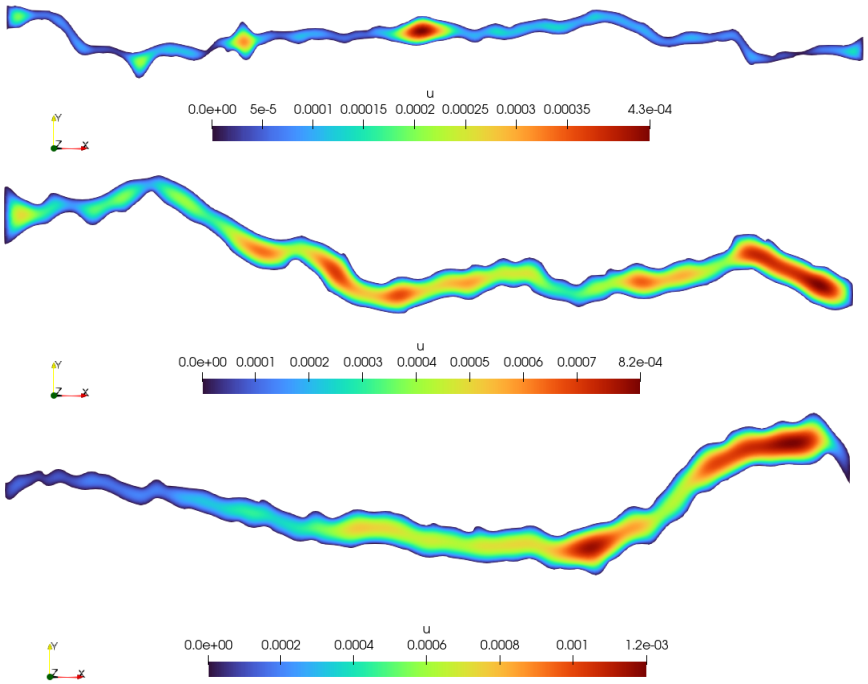


Figure 5. Dimensionless velocity fields computed using the finite element method through `FEniCSx/DolfinX`. The figure displays 2D colormaps of the velocity magnitude u for the six studied apertures. Each image illustrates the spatial distribution of velocity within the fracture geometry, with red regions highlighting areas of peak flow in the fully developed regime.

Table 2. Geometric and hydraulic parameters computed for all apertures using the `FEniCSx/DolfinX` approach.

Aperture	A	p	d_h^*	$\overline{u^*}$	Po	F_{val}
1	0.0599	4.5003	0.0532	8.9e-04	15.9055	1.9882
2	0.1103	4.6984	0.0939	3.4e-04	13.1218	1.6403
3	0.1348	4.5928	0.1742	4.6e-04	14.8588	1.8573

4 Conclusions

This paper presented a Galerkin-based integral (GBI) method for computing dimensionless shape factors in cross-sections bounded by irregular geometries, such as those found in fractured materials. The methodology was applied to real concrete fractures and validated through finite element simulations. The main conclusions are:

- The GBI method successfully computes shape factors for a wide range of irregular aperture geometries at low computational cost. Its ease of implementation and flexibility make it suitable for realistic datasets obtained from experiments or image-based reconstructions.
- The reconstructed velocity fields display physically consistent laminar behavior, with sensitivity to local geometric variations. The use of high-order piecewise polynomial representations ensures accurate modeling of complex fracture boundaries.
- Shape factors obtained using the GBI method closely match those derived from finite element simulations using `FEniCSx/DolfinX`, confirming the accuracy and robustness of the method across different configurations.
- The GBI formulation integrates seamlessly into broader computational workflows for porous and fractured media, offering a reliable and efficient alternative to fully discretized methods for estimating geometric flow resistance.

Acknowledgements. V.A.S.J. acknowledges the Paraíba State Research Support Foundation - FAPESQ (Grant No. 3193/2021) and G.P.O. the Brazilian National Council for Scientific and Technological Development – CNPq for funding this research (Grant No. 405654/2022-7).

Authorship statement. The authors hereby confirm that they are the sole liable persons responsible for the

authorship of this work, and that all material that has been herein included as part of the present paper is either the property (and authorship) of the authors, or has the permission of the owners to be included here.

References

[1] C. A. Issa and P. Debs. Experimental study of epoxy repairing of cracks in concrete. *Construction and Building Materials*, vol. 21, n. 1, pp. 157–163, 2007.
[2] M. A. Abed, J. Fořt, A. Naoulo, and A. Essa. Influence of polypropylene and steel fibers on the performance and crack repair of self-compacting concrete. *Materials*, vol. 14, n. 19, pp. 5506, 2021.
[3] J. Luo, Y. Xie, M. Z. Hou, Y. Xiong, X. Wu, C. T. Lüddeke, and L. Huang. Advances in subsea carbon dioxide utilization and storage. *Energy Reviews*, vol. 2, n. 1, pp. 100016, 2023.
[4] E. Hakami and E. Larsson. Aperture measurements and flow experiments on a single natural fracture. *International Journal of Rock Mechanics and Mining Sciences & Geomechanics Abstracts*, vol. 33, n. 4, pp. 395–404, 1996.
[5] S. R. Brown and C. H. Scholz. Broad bandwidth study of the topography of natural rock surfaces. *Journal of Geophysical Research: Solid Earth*, vol. 90, n. B14, pp. 12575–12582, 1985.
[6] T. Kling, D. Huo, J.-O. Schwarz, F. Enzmann, S. Benson, and P. Blum. Simulating stress-dependent fluid flow in a fractured core sample using real-time x-ray ct data. *Solid Earth*, vol. 7, n. 4, pp. 1109–1124, 2016.
[7] P. C. Carman. Fluid flow through granular beds. *Trans. Inst. Chem. Eng.*, vol. 15, pp. 150–166, 1937.
[8] P. C. Carman. Permeability of saturated sands, soils and clays. *The Journal of Agricultural Science*, vol. 29, n. 2, pp. 262–273, 1939.
[9] K. Yazdchi, S. Srivastava, and S. Luding. On the validity of the carman-kozeny equation in random fibrous media. In *PARTICLES II: proceedings of the II International Conference on Particle-Based Methods: fundamentals and applications*, pp. 264–273. CIMNE, 2011.
[10] W. Sobieski and Q. Zhang. Sensitivity analysis of kozeny-carman and ergun equations. *Technical Sciences/University of Warmia and Mazury in Olsztyn*, vol. 17, n. 3, pp. 235–248, 2014.
[11] N. Srisutthiyakorn and G. M. Mavko. What is the role of tortuosity in the kozeny-carman equation? *Interpretation*, vol. 5, n. 1, pp. SB57–SB67, 2017a.
[12] N. Srisutthiyakorn and G. Mavko. The revised kozeny-carman equation: A practical way to improve permeability prediction in the kozeny-carman equation through pore-size distribution. In *SEG Technical Program Expanded Abstracts 2017*, pp. 3811–3815. Society of Exploration Geophysicists, Tulsa, OK, USA, 2017b.
[13] H. Hoteit and A. Firoozabadi. An efficient numerical model for incompressible two-phase flow in fractured media. *Advances in Water Resources*, vol. 31, n. 6, pp. 891–905, 2008.
[14] O. Al-Hinai, G. Singh, G. Pencheva, T. Almani, and M. F. Wheeler. Modeling multiphase flow with nonplanar fractures. In *SPE Reservoir Simulation Symposium*. OnePetro, 2013.
[15] J. Ding and R. Manglik. Analytical solutions for laminar fully developed flows in double-sine shaped ducts. *Heat and Mass Transfer*, vol. 31, n. 4, pp. 269–277, 1996.
[16] Y.-M. Lee and Y.-M. Kuo. Laminar flow in annuli ducts with constant wall temperature. *International communications in heat and mass transfer*, vol. 25, n. 2, pp. 227–236, 1998.
[17] A. Degheidy, M. Sallah, M. Attia, and M. Atalla. On galerkin method for solving radiative heat transfer in finite slabs with spatially-variable refractive index. *International Journal of Thermal Sciences*, vol. 100, pp. 416–422, 2016.
[18] V. Santos Júnior, A. Lima, S. Farias Neto, I. Gomes, and J. Teixeira. Laminar fluid flow in concentric annular ducts of non-conventional cross-section applying gbi method. *Research, Society and Development*, vol. 10, n. 1, 2021.
[19] V. A. S. Júnior, A. F. S. Júnior, T. A. Simões, and G. P. Oliveira. Poiseuille-number-based kozeny–carman model for computation of pore shape factors on arbitrary cross sections. *Transport in Porous Media*, vol. 138, pp. 99–131, 2021.
[20] V. A. Júnior, S. R. F. Neto, and de A. G. B. Lima. Heat transfer and fluid flow in concentric annular ducts using the galerkin-based integral method: A numerical study. *Diffusion Foundations and Materials Applications*, vol. 30, pp. 53–68, 2022.
[21] Associação Brasileira de Normas Técnicas. NBR 5738: Concrete — Procedure for molding and curing test specimens. ABNT, 2016.